Post-print of: Miszkiel A., Wojciechowski M.: Long range molecular dynamics study of interactions of the eukaryotic glucosamine-6-phosphate synthase with fructose-6-phosphate and UDP-GlcNAc. JOURNAL OF MOLECULAR GRAPHICS & MODELLING. Vol. 78, (2017), s.14-25. DOI: 10.1016/j.jmgm.2017.09.009

Long range molecular dynamics study of interactions of the eukaryotic glucosamine-6-phosphate synthase with fructose-6-phosphate and UDP-GlcNAc

Aleksandra Miszkiel, Marek Wojciechowski

Department of Pharmaceutical Technology and Biochemistry, Gdansk University of Technology, ul. Narutowicza 11/12, 80-233 Gdańsk, Poland

a b s t r a c t

Glucosamine-6-phosphate synthase (EC 2.6.1.16) is responsible for catalysis of the first and practically irreversible step in hexosamine metabolism. The final product of this pathway, uridine 5′ diphospho N-acetyl-d-glucosamine (UDP-GlcNAc), is an essential substrate for assembly of bacterial and fungal cell walls. Moreover, the enzyme is involved in phenomenon of hexosamine induced insulin resistance in type II diabetes, which makes of it a potential target for anti-fungal, anti-bacterial and anti-diabetic therapy.

The crystal structure of isomerase domain from human pathogenic fungus Candida albicans has been solved recently but it doesn't reveal the molecular mechanism details of inhibition taking place under UDP-GlcNAc influence, the unique feature of eukaryotic enzyme. The following study is a continuation of the previous research based on comparative molecular dynamics simulations of the structures with and without the enzyme's physiological inhibitor (UDP-GlcNAc) bound. The models used for this study included fructose-6-phosphate, one of the enzyme's substrates in its binding pocket.

The simulation results studies demonstrated differences in mobility of the compared structures. Some amino acid residues were determined, for which flexibility is evidently different between the models. Importantly, it has been confirmed that the most fixed residues are related to the inhibitor binding process and to the catalysis reaction. The obtained results constitute an important step towards understanding of the inhibition that GlcN-6-P synthase is subjected by UDP-GlcNAc molecule.

Keywords: Glucosamine-6-phosphate synthase UDP-GlcNAc, Molecular dynamics, Cosine content, Mobility analysis

1. Introduction

Glucosamine-6-phosphate (GlcN-6-P) synthase, EC 2.6.1.16, belongs to the glutamine-dependent amidotransferases family. The enzyme uses L-glutamine as a nitrogen donor to catalyse the conversion of fructose-6-phosphate (Fru-6-P) into glucosamine-6-phosphate (GlcN-6-P).

GlcN-6-P synthase is responsible for biosynthesis of important elements of bacterial and fungal cell walls as well as for regulation of glucose metabolism in the hexosamine pathway in the mammalian cells [1]. Thanks to these features, the enzyme seems to be a good target for the antifungal and anti-diabetes treatment [2].

The role of GlcN-6-P synthase in the anti-microbial therapy is based on the selective toxicity phenomenon – inhibiting the enzyme activity in bacterial and fungal cells results in lethal effects while mammalian cells are able to outlive till new copies of the enzyme are produced [3]. As for the role of GlcN-6-P in the anti-diabetes therapy, the enzyme seems to be involved in the hexosamine-induced insulin resistance in type 2 diabetes [4] and in the control of the glucose flux into the hexosamine pathway [5]. For these reasons, studying the molecular mechanisms of its activity regulation is of great importance.

One of the approaches on the way leading to discover the selective method of the activity inhibition of GlcN-6-P synthase could be based on the enzyme regulation by the physiological inhibitor of the eukaryotic enzyme, uridine-5′-diphosphate *N*-acetylglucosamine (UDP-GlcNAc). The compound is the end-product of the hexosamine biosynthetic pathway leading to formation of important elements of fungal cell walls. The first step of this path is catalyzed by GlcN-6-P synthase.

The eukaryotic enzyme (Gfa) shares many features with its prokaryotic counterpart (GlmS), which has been extensively studied [3,6–8]. In both versions, a single subunit contains 2 distinct domains, each one corresponding to one of the steps of

http://dx.doi.org/10.1016/j.jmgm.2017.09.009

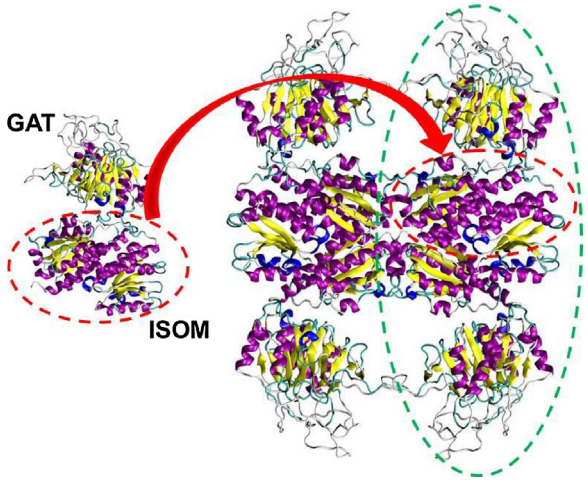

Fig. 1. Structure of GlcN-6-P synthase from *C. albicans*. One of the dimers, corresponding to the prokaryotic structure, is differentiated with the green dashed line.

catalyzed reaction, namely the N-terminal glutamine amidohydrolase (GAT), responsible for glutamine hydrolysis and the C-terminal ketose/aldose isomerase (ISOM) domain, catalyzing the amination and isomerization of Fru-6-P [9]. The bacterial structure of GlcN-6-P synthase is a functional dimer with the glutaminase and isomerase domains connected by a linker and a solvent-inaccessible hydrophobic channel responsible for ammonia transfer from GAT to ISOM domain. As for the eukaryotic counterpart, the crystal structure of the whole enzyme has not been obtained yet; for now only the ISOM domain is available [10]. However, it is known that the whole structure forms a homotetramer also called "dimer of dimers", as each dimer, composed of tight dimers, shows many analogies to the prokaryotic enzyme (Fig. 1). Three main characteristic elements are present in the *C. albicans* structure: the C-terminal and the N-terminal subdomains and the so–called C-tail, encompassing 18C-terminal residues in form of an irregular loop [6]. Within the active site, Glu591, His607 and Lys707 are of particular importance for the catalytic reaction; several other residues, however, are involved in Fru-6-P binding within the active site, i.e. 450–455 which form a loop enclosing the phosphate part of the substrate and stabilize the molecule by forming hydrogen bonds with the phosphate oxygen atoms [11]. One more strategic feature belongs to the ISOM domain: it encompasses the binding site of UDP-GlcNAc, the inhibitor specific to the eukaryotic enzyme. Surprisingly enough, this binding site is not located at the close vicinity of the active center but about 1.5 nm from it.

As GlcN-6-P is a very unstable protein, purification and experimental studies of the enzyme cause many difficulties. Therefore, computational approaches, i.e. molecular modeling tools have been used to succor traditional methods in working on the molecular mechanism of the inhibition under UDP-GlcNAc. As the comparison of crystal structures of the free and inhibitor-bound protein did not reveal any significant differences [10], it is presumed that either it is related to the residues not present in the structure or the essence of the inhibition consists in differences in motions of some elements of the isomerase (ISOM) domain after UDP-GlcNAc binding [10].

Our previous research based on the large-scale molecular dynamics (MD) comparison of the free and inhibitor-bound versions of the enzyme [12] seems to confirm the crucial role of mobility of the ISOM domain fragments, i.e. the C-tail. Rigidification of some strategical regions of the structure, occurring on account of binding of UDP-GlcNAc, could result in disrupting the signal transmission between the enzyme domains and, consequently, lead to the protein's activity inhibition. The following study constitutes a continuation of the previous analysis – in contrast to the prior step, the analyzed systems include the substrate in the active site. The aim of this paper is on one hand to check whether the conclusions made previously prove correct for the structures containing the substrate but also to provide a deeper insight into the influence of the C-tail on the inter-domain signal transmission and on GlcN-6-P synthase inhibition under UDP-GlcNAc.

2. Methods

The main study was based on comparative analysis of 2 trajectories resulting from 300 ns Molecular Dynamics of the ISOM domain of GlcN-6-P synthase from *Candida albicans*. Both simulation systems contained the protein tetramer complexed with the substrate, but only the second included the inhibitor – one molecule of UDP-GlcNAc per each subunit. The trajectory analysis was based on the root mean square fluctuations analysis (RMSF) and the covariance analysis.

2.1. Molecular dynamics setup

The complete crystal structure of the eukaryotic GlcN-6-P synthase has not been solved yet. For now, only the isomerase domain is available, and yet the quality of the model is not perfect – some elements of high mobility, i.e. the C-tail, are not visible [10]. Moreover, the crystal structure of the domain without the inhibitor lacks more fragments than the structure complexed with UDP-GlcNAc. Therefore, both models used in the study were based on the latter crystal structure, taken from the RCSB Protein Data Bank (PDBID: 2PUV). The missing fragments were homology built based on the bacterial structure template (PDBID: 1JXA). All unrequired elements were removed; the initial ligand, 5-amino-5-deoxy-1-o-phosphono-D-mannitol (M6R) was replaced by fructose-6-phosphate (F6R) and polar hydrogens (hydrogen atoms which are parameterized as bonded to electronegative atoms) were added for the hydrogen bond network to be optimized.

The Molecular Dynamics simulations as well as the resulting trajectories analysis were carried out with the Gromacs simulation packages (version 4.5.3 and more recent) [13,14]. Gromos96 subtype 43a2 force field, recommended for simulations of protein systems, has been chosen.

Each of the systems was put into simulation box, which was subsequently filled with pre-equilibrated single point charge (SPC) water molecules [15]. Then, the system's negative charge was neutralized with appropriated number of sodium ions with 0.6 nm as the shortest distance between two entities.

Both systems were energy minimized for 5000 steps of Steepest Descent algorithm. Afterwards, 100 ps position restrained molecular dynamics in the NVT ensemble was performed. During the run all protein's heavy atoms were position restrained with force constant of 1 000 $kJ^x\,mol^{-1x}\,nm^{-2}$ whereas force constant of 50 $kJ^x\,mol^{-1x}\,nm^{-2}$ was used to fix magnesium ions as well as heavy atoms of both ligands.

The actual MD simulations were run for 300 ns in the NPT ensemble at 300 K. The periodic boundary conditions and removal of the center of mass translation were used and the temperature was kept constant at 300 K using Berendsen-thermostat method. The elements of both systems with the substrate were divided into 3 groups: protein, ligands and the rest (water and ions). For each of the groups, the temperature was coupled to a reference temperature bath with the coupling constant of 0.1 ps [15]. The pressure was maintained constant using Berendsen exponential relaxation pressure coupling with time constant of 0.5 ps and the reference pressure of 1 bar [15]. At each step, the vectors of the

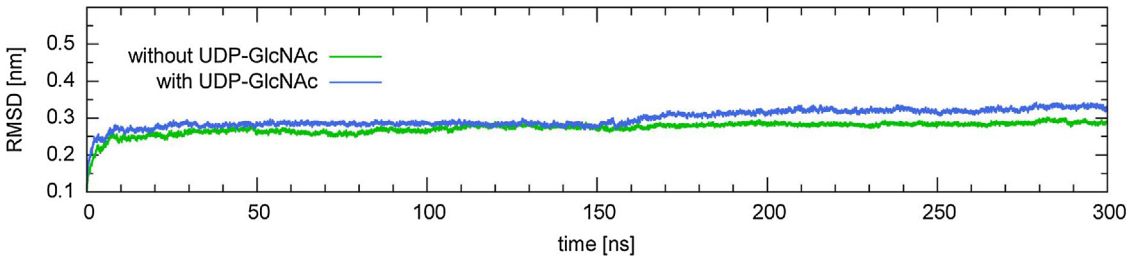

Fig. 2. RMSD time evolution of the inhibitor-free and inhibitor-bound forms of the ISOM domain with respect to the starting structures. Values were calculated every 3 ps and averaged over subunits of the tetramer; only Cα atoms were considered.

simulation box were re-scaled. Initial velocities were randomly generated according to the Maxwell distribution at the temperature of 300 K. The long-range electrostatic interactions were handled by the particle-mesh Ewald (PME) algorithm [16]. Bond lengths were constrained at their optimal values using the LINCS algorithm [17], which allowed a relatively large integration time step of 2 fs to be set.

Since both ligands were not standard molecules such as amino acids or nucleic acids, the GROMACS library did not contain their topologies and therefore, it was necessary to obtain them by other means. The Dundee PRODRG2 [18] server was used for this purpose; thus generated topology was then subjected to modifications according to the parameters of structurally similar molecules from the GROMACS library (nicotinamide adenine dinucleotide, glucose, fructose and uracil) in order to make the final topologies consistent with the chosen force field.

All simulations were run for 150 000 000 steps reaching 300 000 ps (300 ns). The individual systems states comprising coordinates and velocities were collected every 10 000 steps, the energies were saved every 500 steps and the compressed trajectory files were updated every 3000 steps.

2.2. Trajectory analysis

Trajectories resulted from the MD simulations were subjected to several consecutive analyses.

In the first step, the stability of the simulations was confirmed by checking if evolution of parameters such as: energy, root mean square deviation, hydrogen bonds number, radius of gyration, solvent accessible surface and secondary structure of the molecule, did not experience any significant changes during the simulations, which could be a sign of system's disintegration. Also, the distances between ligands and its binding sites were calculated in order to verify if the molecules did not drift away of the protein during the MD. Distances were measured between chosen groups of atoms and compared to analogical distances in the crystal structure (PDBID: 2PUT).

For the substrate, the distance between the mass center of three oxygen atoms of Ser406, Ser452 and Thr455 and the phosphorous atom of the phosphate group from Fru-6-P has been chosen to represent the distance between substrate and its binding site, as it is known that anchoring of the phosphate group to those oxygen atoms is crucial for the ligand positioning [19]. The same distance, measured for the crystal structure and averaged over the subunits, was of 0.108 nm. However, considering that the crystal structure is only a static image of a dynamic protein structure, it can be assumed that the substrate molecule is within the active site if the measured distance is up to 0.150 nm.

For the inhibitor, the distance to its binding site was measured between the least mobile atoms of analyzed groups (the choice was based on the root mean square fluctuations analysis for each of them [data not shown]). The uracyl part of UDP-GlcNAc and the center of three Cα of the most stable residues of the inhibitor binding pocket, were therefore selected. For the crystal structure, that distance was of 0.343 nm, as averaged over subunits.

Table 1
Average root mean square deviation (RMSD) for the inhibitor-free and inhibitor-bound versions of the protein.

Subunit	Inhibitor-free protein				Inhibitor-bound protein			
	A	B	C	D	A	B	C	D
Average RMSD [nm]	0.267	0.279	0.237	0.308	0.291	0.284	0.302	0.314

The trajectories were also checked for convergence by calculating a convergence indicator called cosine-content (cc) [20,21].

The simulations verisimilitude was checked by comparing the values of root mean square fluctuations (RMSF) of the Cα atoms to B-Factor values from the crystal structures. B-Factors, also known as crystallographic temperature factors, constitute a measurement of structure's flexibility. Therefore the correlation between calculated RMSF resulting from MD simulation and experimental B-factors states for the quality and reliability of the simulation.

In order to determine the fragments of the structure which experienced the greatest movement differences, covariance analysis and root mean square fluctuations analysis were used for all Cα atoms of the protein.

3. Results and discussion

While performing the analysis of MD simulation, it is often a point of discussion to what extent the simulation is trustworthy. Two essential questions arise from this: if the simulation run was correct and if the molecule's natural motions were successfully recreated. For those reasons, stability and reliability tests were necessary prior to the proper structural analysis.

3.1. Stability of the systems during the simulation

The first step of performed analysis was a verification if the systems remained stable during the simulation. The visual inspection of proteins' motions in the simulation boxes as well as analysis of the energy evolution [data non shown] did not reveal any significant anomalies. Also, changes of RMSD (Fig. 2 and Table 1), changes of the hydrogen bonds number within the entire protein (Fig. 3) and between each dimer's subunits (Fig. 4), as well as changes of radius of gyration during the MD (Fig. 3), confirmed that both structures remained whole.

Fig. 1 clearly shows that the evolutions of RMSD in both simulations were very stable and similar, especially up to 155th ns of the simulation. The difference noticeable after arises from the evolution of RMSD for subunit D, as shown in Table 1. Detailed analysis of this part of the molecule has not shown any anomalies so it is assumed that the changes are due to a conformational change of very small magnitude, which took place about the 155th ns of the simulation.

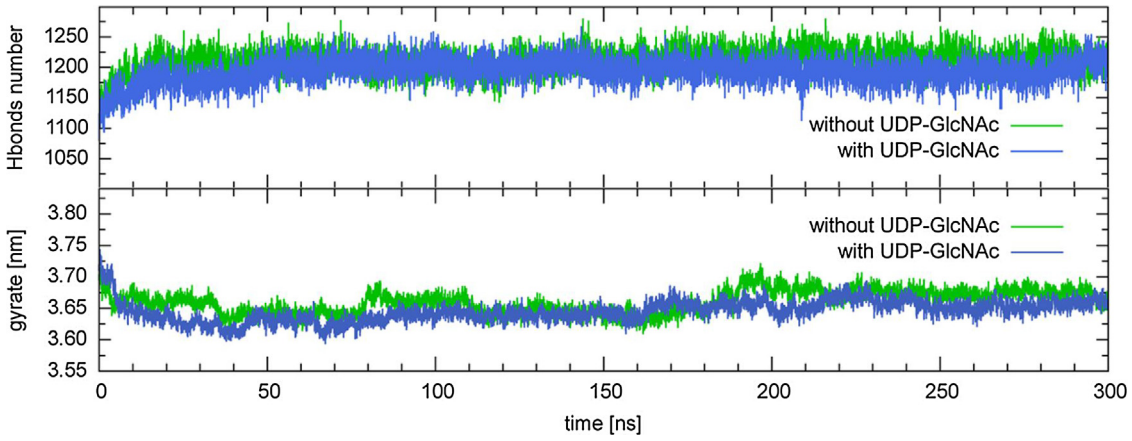

Fig. 3. Time evolution of the total number of hydrogen bonds (above) and of the radius of gyration (below) for the inhibitor-free and inhibitor-bound versions of the protein.

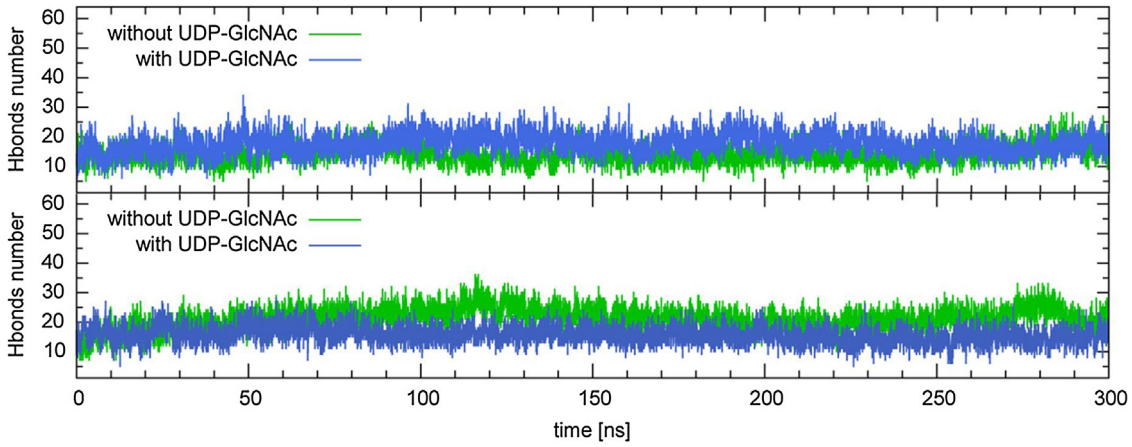

Fig. 4. Time evolution of the number of hydrogen bonds within dimer AB (above) and CD (below) for the inhibitor-free and inhibitor-bound versions of the protein.

The total number of hydrogen bonds in the protein, the time evolution of which is presented in Fig. 3, remained stable (1150–1250) after the first 10 ns of the simulation. As for the evolution of the radius of gyration (Fig. 3), it is less steady for the structure without inhibitor. However, fluctuations calculated in regard to the average value are of very similar values of 2–3%, the difference is then marginal. Starting from the 250th ns the values are slightly, but noticeably (the difference is of about 0.02 nm) greater than for the protein with both ligands. Nevertheless, at the very end of the simulation both lines overlap, which means they converged to the same value of about 3.65 nm.

The evolution of the solvent accessible surface, as well as the secondary structure of the protein over the simulation, have also been studied [data non shown] and did not reveal any anomalies. All performed analyses indicate that both simulations reached stability quite fast and can be regarded as stable starting from about the 20th ns of the simulation.

3.1.1. *Quaternary structure*

The analysis of the total number of hydrogen bonds and of the evolution of the radius of gyration (Fig. 3) showed that the simulated systems did not disintegrate during the molecular dynamics. However, as the quaternary structure, depicted in Fig. 1, is one of the distinctive features of the eukaryotic version of the enzyme, it has been subjected to a more detailed analysis.

The Fig. 4, illustrating the hydrogen bonds number between subunits of both dimers, shows that, in general, there are more discrepancies in the number of hydrogen bonds between subunits of the dimers for the structure without the inhibitor than for its inhibitor-bound counterpart. It can be noticed that the dimer of the subunits C and D in the system without the inhibitor is more hydrogen-bonded not only compared to the dimer AB, but also to any of the dimers of the system containing the inhibitor. However, seeing that the mentioned differences in hydrogen bond number are of relatively small magnitude, they should not affect further analysis.

As for the evolution of the number of hydrogen bonds within a tetramer (between the dimers AB and CD), there is a noticeable difference between compared structures. As shown in Fig. 5, there are more hydrogen bonds between the dimers of the protein with the inhibitor than between the dimers of its inhibitor free analogue.

The analyses of evolution of the number of hydrogen bonds show that the protein with the inhibitor seems more homogeneous than its inhibitor-free counterpart. Furthermore, the general tendency of the protein is to become more compact upon binding of the inhibitor in the substrate presence. Thus, the change in the number of hydrogen bonds between dimers AB and CD noticeable for structure without the inhibitor after the 70th ns of the simulation, (Fig. 5), probably related to the fact that, as it has been mentioned before, the starting structures for both simulations were based on the crystal structure of the protein with UDP-GlcNAc bound, could reflect the real transition taking place for this molecule.

3.1.2. *Distance between protein and ligands*

In order to verify if the ligands remained within their binding pockets during the simulation, distance analyses were performed

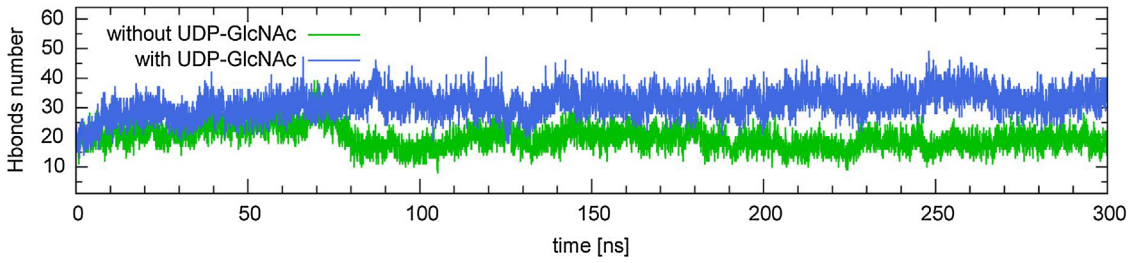

Fig. 5. Time evolution of the number of hydrogen bonds between dimers AB and CD for the inhibitor-free and inhibitor-bound versions of the protein.

for both Fru-6-P and UDP-GlcNAc. All conclusions were confirmed by detailed visual analyses of the ligands' positioning in regard to their binding sites.

3.1.2.1. The substrate (Fru-6-P). The evolution of the substrate distance to the active site during the simulation exhibited important differences between the two versions of the ISOM domain.

In the case of the inhibitor-free complex, only two (A and B) out of four Fru-6-P molecules remained bound to the protein, as shown in Fig. 6 and Table 2. For the subunit A, the average distance was of 0.142 nm which is 0.034 nm higher than the average distance in the crystal structure but still within the acceptable range of phosphorus-oxygen bond. The curve depicted in Fig. 6 reveals that the distance, vaguely fluctuating at the beginning, stabilizes after about 100th ns of the simulation and remains constant at approximately 0.135 nm. Qualitatively similar changes were underwent by subunit B – slightly unstable at the beginning, it mostly stabilized about the 65th ns of the simulation and reached plateau 50 ns later. In contrast to subunit A, the average distance value for subunit B was slightly below the reference (0.101 nm while 0.108 in the crystal structure) therefore there is no shade of doubt that the substrate remained properly bound within the active site. Unlikely the dimer AB, for the subunits of the dimer CD none of the substrate molecules could be considered as correctly positioned, which is clearly visible both on Fig. 6 and Table 2. Although Fru-6-P remained within the pocket for the entire simulation time, which was revealed by visual analysis (data not shown), the phosphate group was too far from the anchoring oxygen atoms, which would make the catalytic activity of the enzyme impossible. In subunit C, at the very end of the molecular dynamics (about the 290th ns), an important shift is observable – the average distance dropped from about 0.350 nm to 0.007 nm, which was related to the ligand reaching the proper position within the active site and the desired bonds between phosphorus atom and the oxygen triad being created. Hence, it can be surmised that for almost entire simulation the substrate was being stabilizing within the pocket. The same tendency, although to the smaller extent, is observable for subunit D. For a longer simulation, it is possible that both ligands from the dimer CD would stabilize after achieving the correct positioning and, therefore, the tetramer would be saturated with four molecules of Fru-6-P, as in the crystal structure.

For the protein with the inhibitor, as depicted in Fig. 6, the evolution of the measured distance did not run in the same manner, although there is a similarity in the fact that two fructose-6-phosphate molecules remained correctly bound to the active site and two others did not. The substrate molecules appertaining to subunits B and C (positioned opposite to each other but not belonging to the same dimer), remained bonded to the anchoring oxygen atoms within the binding pocket, which is confirmed both by the shape of the curves (Fig. 6) and by the average values (Table 2) being 0.110 nm and 0.097 nm for B and C, respectively. The stabilization process was quite fast and after the first 20–30 ns of the simulation, the magnitude of fluctuations decreased distinctly. As for the other two chains, A and D, for both of them the average distance was above the reference value (0.177 nm for A and 0.529 nm for D) but the curves' shape were quite the opposite – for D, the ligand jumped far away from the binding pocket and did not reach any stability throughout the simulation whereas for A it remained stable

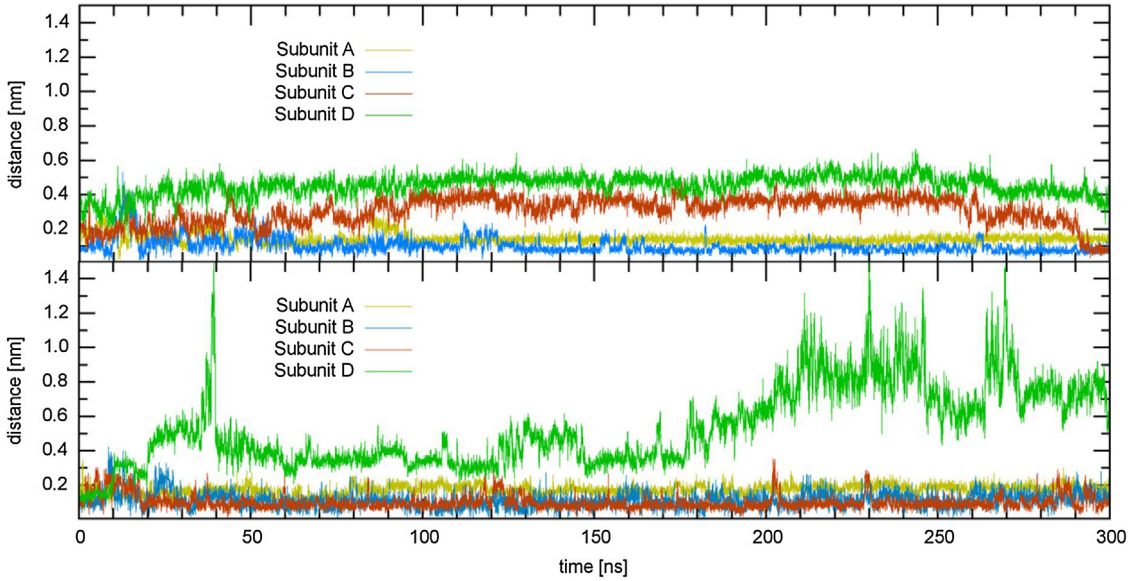

Fig. 6. Time evolution of the distances between the substrate and its binding pocket for each of the subunits of the tetramer for the simulation without the inhibitor (above) and with the inhibitor (below).

Table 2
Distance between the substrate and its binding pocket for the inhibitor-free and inhibitor-bound versions of the ISOM domain.

Subunit/Distance [nm]	Inhibitor-free protein				Inhibitor-bound protein			
	A	B	C	D	A	B	C	D
Min	0.024	0.019	0.032	0.157	0.044	0.04	0.011	0.052
Max	0.304	0.528	0.519	0.664	0.346	0.430	0.350	1.607
Average	0.142	0.101	0.306	0.453	0.177	0.110	0.097	0.529

and buried within the pocket but did not achieve the positioning allowing to create the required anchoring bonds. Alike chain D for the inhibitor-free domain, it is possible that the substrate would attain the desired pose if the molecular dynamics were longer.

3.1.2.2. The inhibitor (UDP-GlcNAc). For the inhibitor, the average distances, measured between the uracyl part and the center of three Cα of the least mobile residues of the inhibitor binding site, were of 0.457 nm, 0.356 nm, 0.388 nm and 0.302 nm for subunits A, B, C and D, respectively. As shown in Fig. 7, for the subunits: A, B and D the distances did not change much during the simulation. However, the average distance for the subunit A was above the reference from the crystal structure (0.343 nm). The Fig. 7 as well as the visual analysis confirmed that at the very beginning of the simulation, the ligand moved from its binding site, found a new stable position and remained there till the end of molecular dynamics. Thus, it must be noticed that the inhibitor was not fulfilling its role for that subunit. As for the subunit C, it is clearly visible on Fig. 7 that an abrupt change occurred at the 236th nanosecond of the simulation – the distance increased for more than 0.2 nm. The visual analysis of this fragment of the simulation confirmed that this transition accounted for the inhibitor drifting away from the binding pocket.

Therefore, for any analysis including the inhibitor presence, the subunit A should be excluded, as well as the last fragment of 70 ns for the subunit C.

Concerning the distances between both ligands and the protein, for now, there is no experimental evidence confirming that in physiological conditions, the eukaryotic GlcN-6-P synthase enzyme simultaneously binds four substrate molecules or four inhibitor molecules. It looks this way for the crystal structure [10] but one should consider that those crystals were obtained by saturation of the enzyme so they do not necessary correspond to cellular reality.

Thus, it is possible that the observed phenomena are not anomalies and reveal the actual state of the liganded enzyme on the given extent of time. However, for the study to be accurate, the subunits devoid of the substrate were not taken into account for all analyses concerning interactions between the protein and the substrate. Likewise, subunits where UDP-GlcNAc was not properly bound were not taken into account for the analysis of interactions between protein and inhibitor.

3.2. Verisimilitude of the simulations

As mentioned before, the verisimilitude of a simulation can be estimated by comparing root mean square fluctuations to B-Factor values of the crystal structure.

Fig. 8 clearly shows that the RMSF curves are very much in line with the B-Factor graph. The perfect overlapping of several fragments of the domain i.e. 390–400 or 510–520 indicates that, despite the existence of obvious differences, due to protein's dynamics along the simulation, the motions on selected ranges reflect the reality to a satisfying degree. Therefore, both performed molecular dynamics seem reliable.

Moreover, it is clearly visible that the RMSF values are much more consistent with the B-Factors of the crystal structure containing the ligands (PDBID: 2PUV) than with the structure of the free protein (PDBID: 2PUW). This observation is not particularly surprising as both simulations were based on the modified model of the complexed structure (which had a much better resolution).

One should also notice that all B-Factor values of the free structure are in general greater than of its complexed counterpart (see y2 axes in Fig. 8), which proves a greater mobility of this model and could be the direct reason why many of its fragments are not being present in the crystal structure.

Despite of the missing data for some of the residues in the crystal structure, it may be acknowledged that the quality of the protein's motions' mapping is very good for both simulations. Thus, their verisimilitude has been confirmed.

3.3. Convergence of the trajectories

In order to make sure that the analyzed trajectories were describing global motions, related to the protein's physiological function, instead of irrelevant and chaotic oscillations, convergence analysis was performed for both trajectories.

The range 140–300 ns was found to be the longest fragment reaching the end of the trajectory and fulfilling the convergence condition for the whole protein and for each subunit separately. However, it is worth mentioning that, as it turned out, the remaining range 0–140 ns, coinciding with the stabilization stage, was also fulfilling the cc criterion, which means that the stabilization phase,

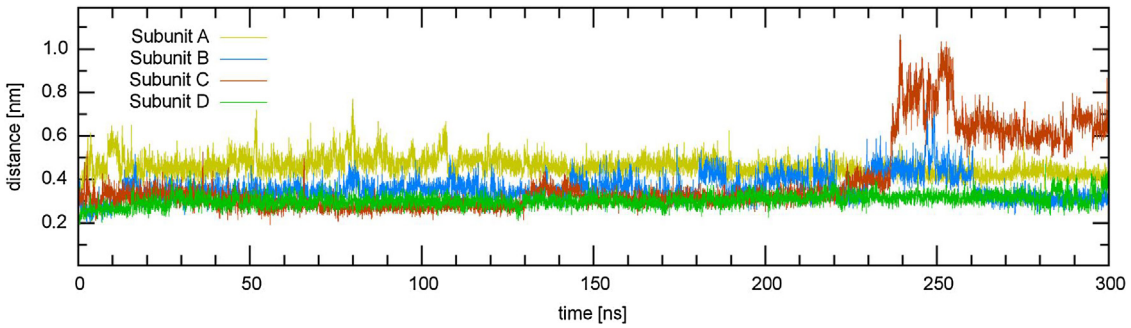

Fig. 7. Time evolution of the distances between the uracyl part of the inhibitor and Cα atoms of the three selected residues from the inhibitor binding site for each of the subunits of the tetramer.

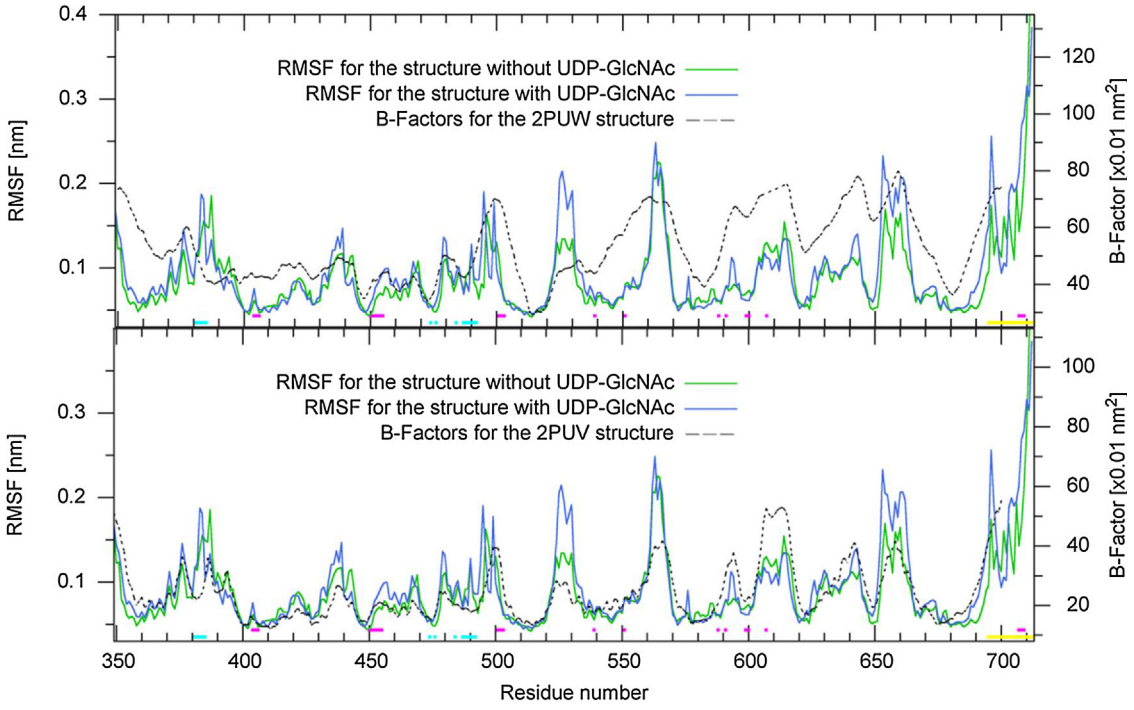

Fig. 8. Comparison of RMSF values calculated for the inhibitor-free and inhibitor-bound versions of the ISOM domain to BFactor values from the crystal structure without (2PUW) and with the ligands (2PUV). Only Cα were considered for the analysis. The results were averaged over the subunits of the tetramer. Cyan horizontal bar corresponds to the inhibitor binding site, magenta – amino acids of the active center, yellow – the C-tail. BFactors for the residues non visible in the crystal structure are ommited. (For interpretation of the references to colour in this figure legend, the reader is referred to the web version of this article.)

Table 3
Cosine content values of the first eigenvector for the selected range (140–300 ns) and for the rest of the trajectory (0–140 ns) of both simulations of the inhibitor-free (above) and inhibitor-bound (below) versions of the protein.

Subunit/ Range [ns]	protein	A	B	C	D
0–140	0.319	0.272	0.021	0.095	0.254
140–300	0.439	0.467	0.405	0.229	0.410
Subunit/ Range [ns]	protein	A	B	C	D
0–140	0.069	0.417	0.007	0.002	0.019
140–300	0.359	0.482	0.096	0.235	0.488

although quite long, was relatively orderly and devoid of chaotic oscillations.

The cc values of the first principal components for both: the selected range and the rest of the trajectory, are presented in Table 3. All values are below 0.5 which, for the structure of this size, can be sign of good sampling of the potential energy hypersurface. Comparison of the RMSF values, calculated for the selected range, constitute the basis of the mobility analysis performed in the second step of the MD results' analysis.

3.4. Mobility analysis

The analyses of differences in mobility of particular amino acids were used to reveal the influence of the inhibitor binding upon the presence of the substrate (Fig. 9). Moreover, additional tests involving the previously obtained trajectories for the structures with no Fru-6-P bound were run in order to show the sole influence of the substrate binding on the structure's mobility (Figs. 10 and 11).

As shown in Figs. 9–11, comparisons of the trajectories revealed some regions on which the curves were practically overlapping (505–520, 540–550). On the other hand, significant differences are noticeable for some other fragments of the structure, namely the functionally important parts of the protein, such as the active site, the inhibitor binding pocket and the C-tail.

As can be seen in Fig. 11, binding of each of the ligands separately to the free ISOM domain had similar consequences on its mobility – the N-part of the structure and part of the C-tail have become less mobile. This can suggest that the rigidification noticed is related to appearance of some new hydrogen bonds and salt bridges upon binding of a ligand and not to the characteristics of this particular molecule. Reports referring to the bacterial version of GlcN-6-P synthase inform that the protein become noticeably more ordered upon substrate binding, and this observation is particularly visible for the C-tail, which is completely unordered in the free model and forms a regular loop only while Fru-6-P is present [22]. Thus, the observation described could be of similar basis and prove the correct imaging of the structure's behavior towards the substrate.

3.4.1. Inhibitor and substrate binding sites

The UDP-GlcNAc (inhibitor) binding pocket is built of residues: 381–388, 474, 476, 484 and 487–492, while the Fru-6-P (substrate) binding site comprises the residues: 403–406, 450–455, 501–503, Leu539, Leu551, Lys588, Glu591, Gly599, Val600, His607# and Lys707.

As shown in Figs. 9–11, binding of the substrate seems to have stabilizing effect on the active site – all residues which are responsible for the substrate binding as well as Lys707 (belonging to the C-tail), became more stable. On the other hand, binding of the inhibitor upon the substrate presence caused very little change to the fluctuations of most of the residues building the active site (Fig. 9). Excepting residue Lys707, for which an important mobility increase was noticed, the only residues affected (and to a much lesser extent) were: the fragment 450–455, constituting a loop encompassing the phosphorous part of the substrate. By contrast, residues Val501 and His607# became rigidified upon the inhibitor binding. The later residue belongs to the neighboring subunit and is of key importance for the catalytic reaction. It is worth mention-

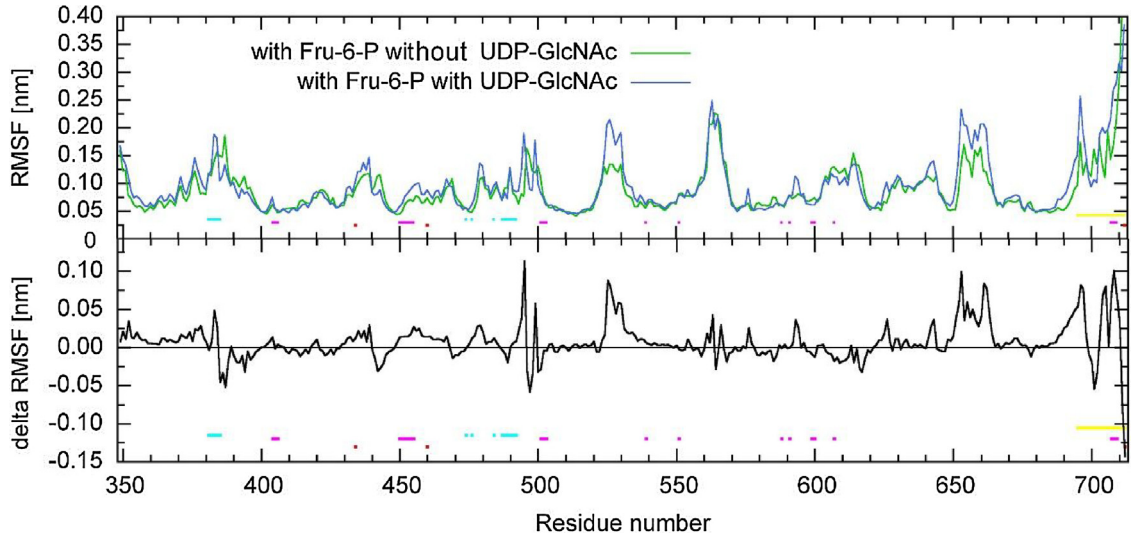

Fig. 9. Comparison of RMSF values (above) and RMSF differences (below) calculated for the inhibitor-free and inhibitor-bound versions of the ISOM domain. The difference is positive if a residue has become more mobile upon inhibitor binding and negative if the opposite. The analysis was made on the range 140–300 ns; only Cα atoms were considered for the analysis. Results were averaged over subunits A and B for the inhibitor-free protein, and over subunits B and C for the inhibitor-bound protein. Cyan horizontal bar corresponds to the inhibitor binding site, magenta – residues of the active center, yellow – the C-tail. (For interpretation of the references to colour in this figure legend, the reader is referred to the web version of this article.)

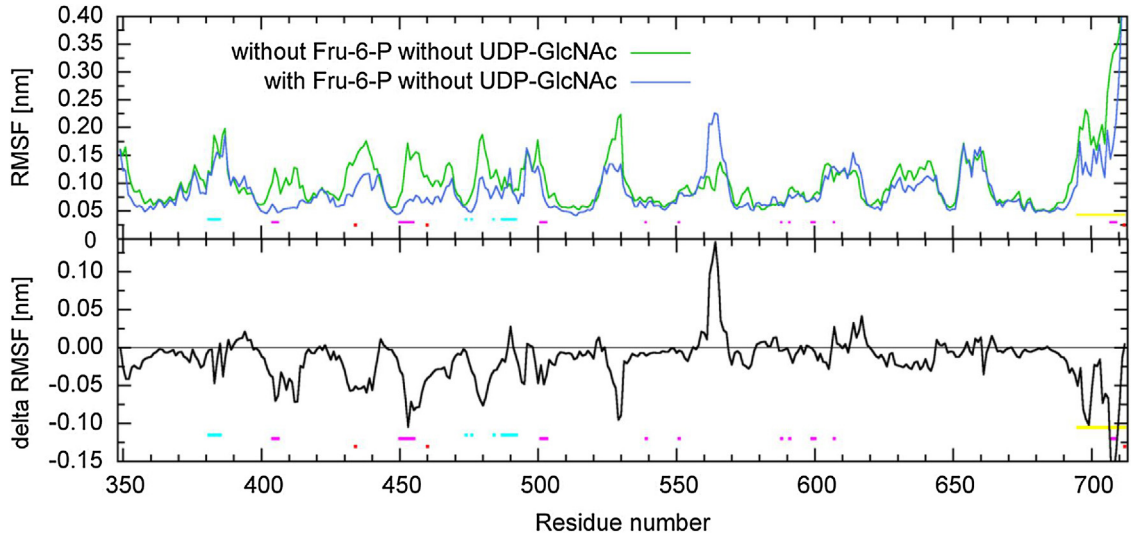

Fig. 10. Comparison of RMSF values (above) and RMSF differences (below) calculated for the inhibitor-free versions of the protein without and with the substrate. The difference is positive if a residue has become more mobile upon substrate binding and negative if the opposite. The analysis was made on the range 145–300 ns for the protein without the substrate and on the range 140–300 ns for the protein with the substrate; only Cα atoms were considered for the analysis. Results were averaged over the tetramer for the protein without the substrate and over subunits A and B for the protein with the substrate. Cyan horizontal bar corresponds to the inhibitor binding site, magenta – residues of the active center, yellow – the C-tail. (For interpretation of the references to colour in this figure legend, the reader is referred to the web version of this article.)

ing that it can only fulfill its role while both subunits are correctly positioned towards each other in the dimer [10]. Comparison of RMSF values for the domains containing and non-containing the inhibitor (Fig. 9) showed that the mobility of this residue decreased upon UDP-GlcNAc binding. What's interesting, rigidification does not result from binding of the substrate itself as the latter results rather in mobility increase than decrease (Fig. 10). This suggests that the change noticed for His607# is related to the inhibitor and, considering the residue's role in the mechanism of the catalyzed reaction, it can have influence on the inhibition process due to UDP-GlcNAc presence. It is worth mentioning that these results are consistent with the observations described by Raczynska et al., according to which in the crystal structures of the ISOM domain from C. albicans, the residue His607# is either completely (in the structures without the inhibitor) or partly (in the structures with the inhibitor) invisible, where the only visible residues are inactive – too far from the active site.

3.4.2. *The C-tail*

In all performed simulations, the C-tail was the most motile fragment of the ISOM domain, which is clearly visible in Figs. 8–11. Amongst the residues forming the C-tail, the greatest change concerned Lys707. As this residue is directly involved in the process of substrate binding, this observation seems consistent with the results described for the ISOM domain of the *E. coli* GlcN-6-P synthase, for which a significant ordering of the C-end residues has been noticed [22]. It should be specified, however, that despite the putative analogy, the extent of this phenomenon would have to be

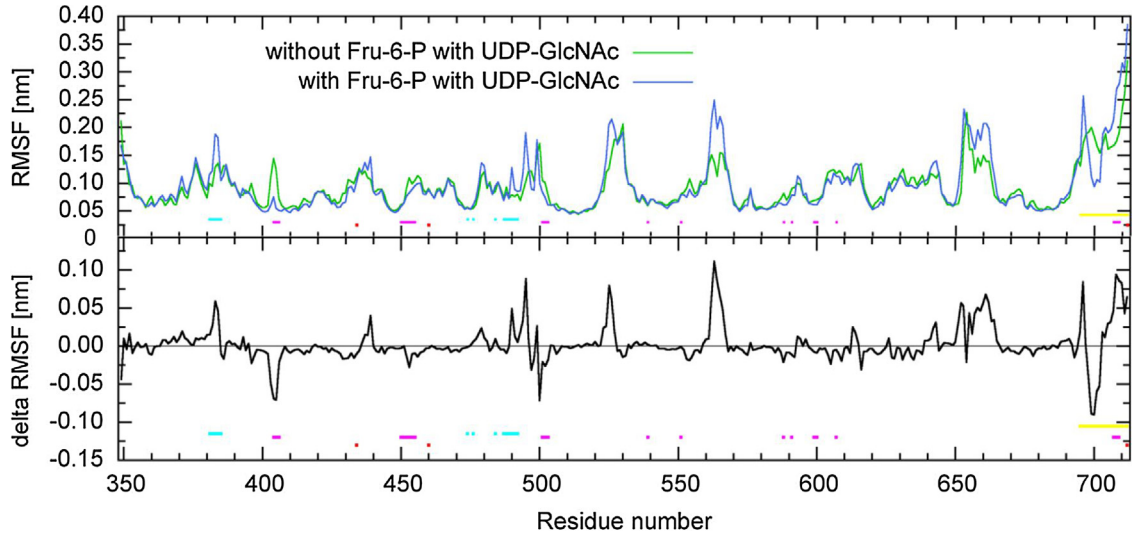

Fig. 11. Comparison of RMSF values (above) and RMSF differences (below) calculated for the inhibitor-bonded versions of the protein without and with the substrate. The difference is positive if a residue has become more mobile upon substrate binding and negative if the opposite. The analysis was made on the range 145–300 ns for the protein without the substrate and on the range 140–300 ns for the protein with the substrate; only Cα atoms were considered for the analysis. Results were averaged over the tetramer for the protein without the substrate and over subunits B and C for the protein with the substrate. Cyan horizontal bar corresponds to the inhibitor binding site, magenta – residues of the active center, yellow – the C-tail. (For interpretation of the references to colour in this figure legend, the reader is referred to the web version of this article.)

different – on the contrary to the C. albicans enzyme, the C-tails from the *E. coli* protein are perfectly visible in the crystal structure. This suggests that the degree of the C-tails' rigidification in the eukaryotic enzyme is much smaller than in its bacterial analogue [10] and, itself, is not sufficient to make these fragments visible in the crystallographic experiments.

The C-tail's mobility has also experienced significant changes. upon binding of UDP-GlcNAc. The character of these differences, however, was non-homogenous: residues Asp700 and Glu712, corresponding to the C-tail's extremes, have been stiffened whereas the inner part have become considerably more motile. The key to explain these discrepancies could be the residue Lys707, which belongs to the residues involved in binding of the substrate inside the active site. It is located in the middle part of the C-tail, thus while the ligand is binding, new bonds are being created in that specific area, which becomes more rigidified then the other parts of the molecule (Fig. 10).

On the other hand, as mentioned earlier, when the inhibitor is binding to the substrate-protein complex, an increase in mobility of the residues building the active site, especially Lys707, can

```
GFPT1_HUMAN  333 IMKGNFSSFMQKEIFEQPESVVNTMRGRVNFDDYTVNLGGLKDHIKEIQRCRRLILIACG 392
GLMS_ECOLI   243 GDKGIYRHYMQKEIYEQPNAIKNTLTGRISHGQVDLSELGPN-ADELLSKVEHIQILACG 301
GFA1_CANAL   345 IMKGPYKHFMQKEIFEQPDSAFNTMRGRIDFENCVVTLGGLKSWLSTIRRCRRIIMIACG 404
                   ** :  :*****:***::  **: **:.. :  :.  * :   . : : .:: ::***

GFPT1_HUMAN  393 TSYHAGVATRQVLEELTELPVMVELASDFLDRNTPVFRDDVCFFLSQSGETADTLMGLRY 452
GLMS_ECOLI   302 TSYNSGMVSRYWFESLAGIPCDVEIASEFRYRKSAVRRNSLMITLSQSGETADTLAGLRL 361
GFA1_CANAL   405 TSYHSCLATRSIFEELTEIPVSVELASDFLDRRSPVFRDDTCVFVSQSGETADSILALQY 464
                 ***.: :.:*  :*.*: :*  **:**:*  *.: * *:.  . :********:: .*:

                 ............................................................

GFPT1_HUMAN  571 EGALKIKEITYMHSEGILAGELKHGPLALVDKLMPVIMIIMRDHTYAKCQNALQQVVARQ 630
GLMS_ECOLI   481 EGALKLKEISYIHAEAYAAGELKHGPLALIDADMPVIVVAPNNELLEKLKSNIEEVRARG 540
GFA1_CANAL   584 EGALKIKEISYMHSEGVLAGELKHGILALVDEDLPIIAFATRDSLFPKVMSAIEQVTARD 643
                 *****:***:*:*:*.  ******* ***:*  :*:* .  .:    *  . :::* **

GFPT1_HUMAN  631 GRPVVICDKEDTETI-KNTKRTIKVPHSVDCLQGILSVIPLQLLAFHLAVLRGYDVDFPR 689
GLMS_ECOLI   541 GQLYVFADQDAGFVSSDN-MHIIEMPHVEEVIAPIFYTVPLQLLAYHVALIKGTDVDQPR 599
GFA1_CANAL   644 GRPIVICNEGDAIISNDKVHTTLEVPETVDCLQGLLNVIPLQLISYWLAVNRGIDVDFPR 703
                 *:  *:.::       .:    :::*.  : :  :: .:****::: :*: :* *** **

GFPT1_HUMAN  690 NLAKSVTVE 698
GLMS_ECOLI   600 NLAKSVTVE 608
GFA1_CANAL   704 NLAKSVTVE 712
                 *********
```

Fig. 12. Multiple sequence alignment (MSA) of GlcN-6-P isomerase domains from human, *C. albicans* and *E. coli* cells. The C-tail is highlighted in yellow; Glu608, amino acids forming the C-tail lock as well as the position important for the steric hindrance removal are represented in red; Asp596 and the residues forming the P-loop-like structure and immobilizing the N-terminal part of the C-tail are shown in green.

be noticed. This is observable both in Figs. 9 and 10. Considering that stability of a binding pocket is necessary for the ligand binding, it can be assumed that an increase in mobility of the residues forming the active site disrupts the substrate binding. Although this assumption is not confirmed by the crystal structure [10], the authors of the experiment admit themselves that not all the aspects of the enzyme activity have been explained, which leaves some place for speculations and predictions related, among others, the process of inhibition occurring upon binding of UDP-GlcNAc.

Anyway, the increase in mobility of Lys707 and the decrease in mobility of the four neighboring residues, responsible for the communication and signal transferring between both domains of the enzyme, seem to confirm the hypothesis of the inhibition upon UDP-GlcNAc binding, proposed in our previous paper [12], related to interfering with the signal transfer via the C-tail, as well as destabilization of the active site upon the inhibitor binding.

3.4.3. *The C-tail lock*

The conclusion drawn above, concerning the significance of the C-tail's mobility changes for the GlcN-6-P synthase activity modulation, provoked further research on this part of the enzyme's structure.

Multiple sequence alignment of GlcN-6-P synthase isomerase domains from prokaryotic and eukaryotic sources (Fig. 12) revealed some interesting, distinct features of both versions of the enzyme. As for the bacterial protein, at the very beginning of the domain, a small, positively charged pocket can be identified, formed by a couple of well conserved residues. Namely, the side chains of Lys245 and His250, as well as the inward-pointing backbone amine groups of residues: Tyr251, Met252, Gln253, shape the P-loop-like structure, able to bind negatively charged groups (Fig. 14). Particularly, the mentioned amide groups are located at the N-terminus of the alpha helix – just like in a regular P-loop. Interestingly, it is not the phosphate group that is bound by this structure, but the carboxyl moiety of the Asp596 sidechain. This particular residue is very well conserved in sequences of GlcN-6-P synthases and since it is located at the opposite, C-terminal end of the chain, this interaction results in a compact structure with the C- and N-terminal parts zipped together. The remaining 12 amino acids of the chain form the C-tail, having a form of an irregular loop, and covering the Fru-6-P binding site like a lid.

The C-terminal residue of this loop, which is Glu608, is located on the opposite side of the binding pocket; some interesting differences between prokaryotic and eukaryotic structures can be identified for this particular amino acid as well. For the structure from *E. coli*, the position of the residue is locked by two salt bridges, formed by interactions of Glu608 with the sidechains of Lys503* and Arg331. This residues form the "lock" immobilizing the C-tail (Fig. 13).

On the other hand, in the enzymes of eukaryotic origin, the Arg331 residue is replaced with Leu – thus an important element of the C-tail lock is missing (Fig. 12). This way, mobility of the C-tail in the human and *C. albicans* versions of GlcN-6-P synthases is less restricted than the C-tail's mobility in the prokaryotic organisms. It is worth mentioning that the enzymes from these two eukaryotic organisms are susceptible to feedback inhibition by UDP-GlcNAc whereas the enzyme from *E. coli* is not. Thus, the lack of the lock may condition the degree of mobility of the C-tail and its susceptibility to mobility changes upon the inhibitor binding.

To verify this hypothesis, a mutated version of the *C. albicans* receptor with the C-tail lock introduced (Leu434 – the *C. albicans* counterpart of Arg331 in *E. coli* – was replaced with Arg) was prepared in order to check if this change would decrease the mobility of the C-tail.

In order to extract the range of the trajectory describing the physiologically relevant, global motions of the protein, the convergence analysis was performed. The range 145–300 ns was found to be the longest fragment reaching the end of the trajectory and fulfilling the convergence condition with cc values of 0.495, 0.182, 0.419, 0.404 and 0.000 for the whole molecule and separate subunits, respectively.

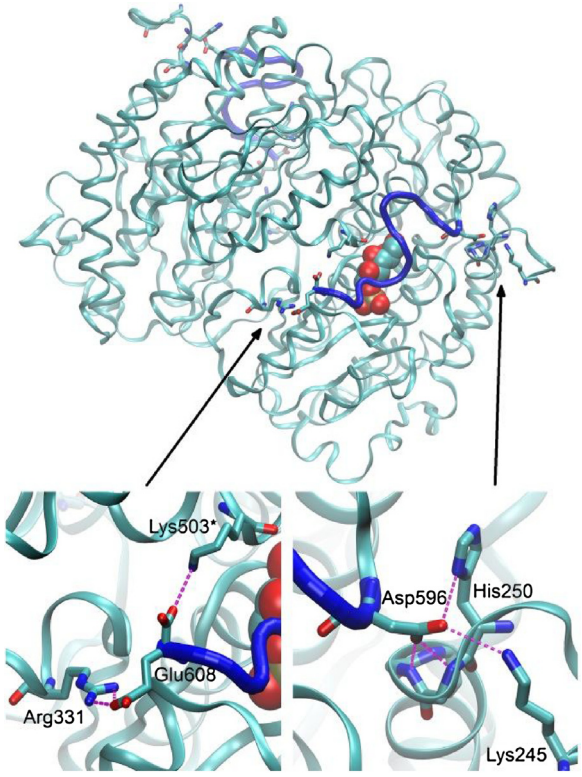

Fig. 13. Dimer of *E. coli* GlcN-6-P isomerase domains based on 1jxa PDB structure. N-terminal part of the chain forming the C-tail is shown as a blue tube. Ligand in the active site is shown as CPK model. At the bottom, close-ups to the beginning (right) and the end (left) of the C-tail are presented. For picture clarity, only the backbone atoms of residues Tyr251, Met252 and Gln252 comprising the N-terminus of the first alpha-helix in this domain, are shown. (For interpretation of the references to colour in this figure legend, the reader is referred to the web version of this article.)

As the model did not contain any ligand bound, in the further analyses the trajectory was compared to its native analogue, which had been obtained and analyzed in our previous study.

As depicted in Fig. 14, the mutation affected the protein's mobility causing rigidification in almost all the structure. As expected, the phenomenon was especially noticeable for the C-tail – the average RMSF values for these residues decreased of about 0.15-0.20 nm.

The mutation-induced mobility changes compared to the same phenomenon caused by the inhibitor binding (Fig. 15), brings interesting observations. In both cases, most of the structure was rigidified to almost the same degree. However, as deduced from the amplitude of RMSF changes, the influence of mutation was significantly stronger for several regions, including the C-tail. Thus, one could conclude that the C-tail lock introduction would have a similar impact on the enzyme's mobility as binding of the inhibitor.

The significance of the C-tail lock's presence to the C-tails's immobilization is also apparent when comparing crystal structures of prokaryotic (PDBID: 1MOS) and eukaryotic (PDBID: 2PUV) ISOM domains. For the *C. albicans* version, where the C-tail lock is missing, the part of the domain's chain located after the P-loop like lock (all residues after Asp700), were not visible in the experiment and thus are not present in the PDB file, whereas for the *E. coli* version, where the C-tail lock is functioning by fastening the C-tail, the complete structure could be solved.

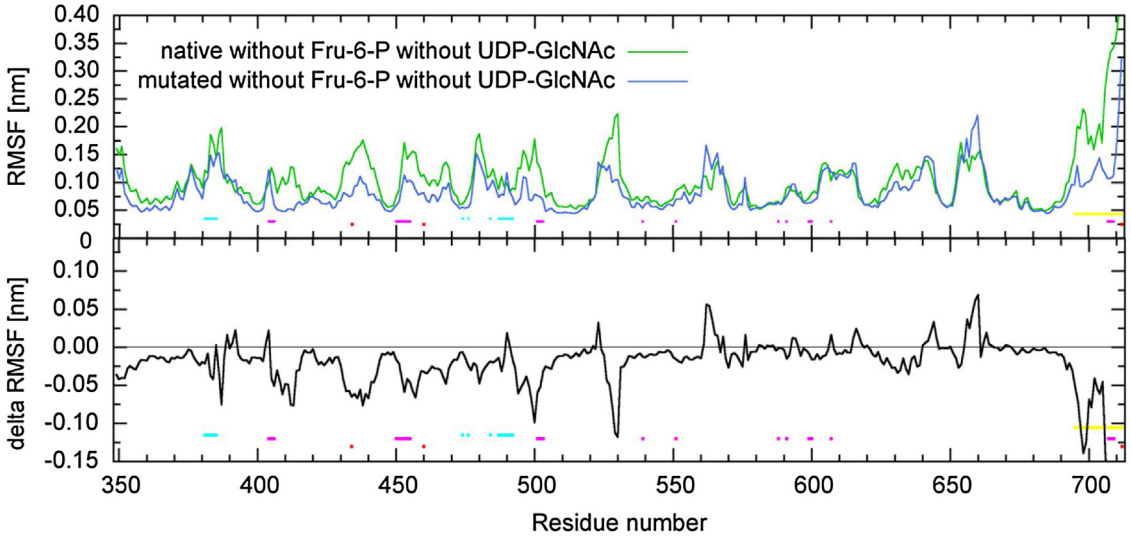

Fig. 14. Comparison of RMSF values (above) and RMSF differences (below) calculated for the native and mutated versions of the protein without any ligands. The difference is positive if a residue has become more mobile upon the mutation and negative if the opposite. The analysis was made on the range 145–300 ns; only Cα atoms were considered for the analysis. Results were averaged over the tetramer. Red points correspond to the mutations, cyan horizontal bar – to the inhibitor binding site, magenta – amino acids of the active center, yellow – the C-tail. (For interpretation of the references to colour in this figure legend, the reader is referred to the web version of this article.)

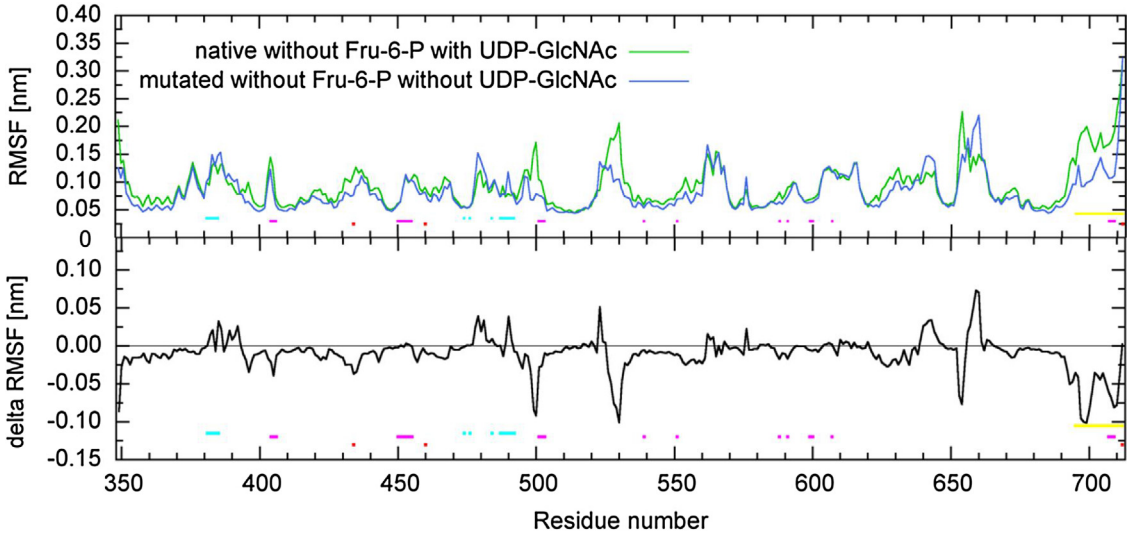

Fig. 15. Comparison of RMSF values (above) and RMSF differences (below) calculated for the native and mutated versions of the protein with the inhibitor bound. The difference is positive if a residue has become more mobile upon the mutation and negative if the opposite. The analysis was made on the range 145–300 ns; only Cα atoms were considered for the analysis. Results were averaged over the tetramer. Red points correspond to the mutations, cyan horizontal bar – to the inhibitor binding site, magenta – amino acids of the active center, yellow – the C-tail. (For interpretation of the references to colour in this figure legend, the reader is referred to the web version of this article.)

This observations suggest that the hypothesis of the C-tail's mobility diminution, resulting from the mutation is an interesting subject for further investigation and could be confirmed by a laboratory experiment.

4. Conclusions

The foregoing study is a continuation of the previous research, extended to include models of the protein with the substrate present in the enzyme binding pocket.

The reaction catalyzed by GlcN-6-P is quite complex and requires precise and accurate order of substrate binding. L-Glutamine can be bound to the GAT domain only if Fru-6-P is correctly positioned within its binding pocket, located in the ISOM domain. Thus, an inter-domain communication system is necessary to transfer conformational changes triggered in the ISOM domain upon Fru-6-P binding to the GAT domain. It was confirmed that such a system exists for the bacterial version of the enzyme [23]. As for the eukaryotic protein, it is known that the quaternary structure of the ISOM domain, especially the interactions within a functional dimer, condition the way of ligands' binding. Moreover, the C-tail, and particularly its few terminal residues, play the key role in the communication and signal transferring between the enzyme domains – deletion of this fragment strongly disrupts both these processes. On the other hand, it had been previously shown that UDP-GlcNAc binding inhibits glutamine hydrolysis and, in consequence, the GlcN-6-P synthetic activity of the whole enzyme whereas no effect was detected on glutamine hydrolysis by the isolated GAT domain and on hexose phosphate isomerization by the isolated ISOM domain [24]. This observation clearly suggests that

GlcN-6-P synthase's activity inhibition upon UDP-GlcNAc binding results from disruption of the interdomain communication, rather than from changes in any of the two domains alone. Since the C-tail is an important element of the ammonia channel and interdomain interface, any alterations of its mobility must interfere with the interdomain communication and thus show as the enzyme's activity changes.

One of the main differences between crystal structures of the prokaryotic and eukaryotic versions of GlcN-6-P synthase is the C-tail's presence. For this fragment to be visible in the crystal structure, it should be completely ordered – not only the substrate binding within the active site, but also the C-tail lock's presence is required. In the *E. coli* version, it is known that upon Fri-6-P binding, the C-tail, which forms the major part of the ammonia channel walls, becomes ordered and covers the synthase site [22], which makes it visible in the crystal structure. As for the *C. albicans* counterpart, the same phenomenon seems to be observed, but to a considerably lesser extent; binding of the substrate rigidifies the C-tail but, as there is no C-tail lock, the degree is not sufficient for the C-tail to become completely ordered and, for that reason, this fragment would not be present in the crystal structure. However, it seems highly possible that in the mutein described herein, the whole C-tail would be visible.

As a continuation of our previous study, the results obtained herein confirm the existence of important discrepancies in the structure's mobility also between MD simulations of the models with bound substrate, of which the only difference is the inhibitor presence. In this case, binding of the inhibitor provokes mobility increase for the residues building the substrate active site, including the middle part of the C-tail. On the other hand, the C-tail's both ends are being rigidified thus this part of the structure is locked in form of a very mobile loop, clipped from both sides. This way, mobility changes induced by inhibitor binding, can strongly interfere with the signal transferring between domains, causing the enzyme's activity loss.

As the matter of fact, UDP-GlcNAc can be regarded as the GlcN-6-P synthase's activity modulator, functioning by inducing changes in the mobility of the residues participating in the interdomain signal transfer. The presented results of *in silico* experiments also suggest that similar changes can be caused by the presence of the C-tail lock in the ISOM domain's structure. Planned laboratory experiment involving the *C. albicans* version of the enzyme with artificially introduced C-tail lock can shed additional light to the mechanism of GlcN-6-P synthase inhibition by UDP-GlcNAc and validate presented hypothesis about significance of the C-tail's mobility changes in this process

Acknowledgements

This research was supported in part by TASK (the Academic Computer Centre in Gdansk). The authors thank TASK for providing computing resources and acknowledge the financial support of the Polish Ministry for Science and Higher Education.

This research was supported in part by PL-Grid Infrastructure.

References

[1] M. Buse, Hexosamines, insulin resistance, and the complications of diabetes: current status, Am. J. Physiol. 290 (2006) 1–15.
[2] E. Borowski, Novel approaches in the rational design of antifungal agents of low toxicity, Farmaco 55 (2000) 206–208.
[3] S. Milewski, Glucosamine-6-phosphate synthase–the multi-facets enzyme, Biochim. Biophys. Acta 1597 (2002) 173–192.
[4] L.F. Hebert, M.C. Daniels, J.X. Zhou, E.D. Crook, R.L. Turner, S.T. Simmons, J.L. Neidigh, J.S. Zhu, A.D. Baron, D.A. McClain, Overexpression of glutamine:fructose-6-phosphate amidotransferase in transgenic mice leads to insulin resistance, J. Clin. Invest. 98 (1996) 930–936.
[5] D.A. McClain, E.D. Crook, Hexosamines and insulin resistance, Diabetes 45 (1996) 1003–1009.
[6] A. Teplyakov, G. Obmolova, M. a Badet-Denisot, B. Badet, I. Polikarpov, Involvement of the C terminus in intramolecular nitrogen channeling in glucosamine 6-phosphate synthase: evidence from a 1.6 angstrom crystal structure of the isomerase domain, Struct. Fold. Des. 6 (1998) 1047–1055.
[7] A. Teplyakov, G. Obmolova, B. Badet, M.A. Badet-Denisot, Channeling of ammonia in glucosamine-6-phosphate synthase, J. Mol. Biol. 313 (2001) 1093–1102.
[8] P. Durand, B. Golinelli-Pimpaneau, S. Mouilleron, B. Badet, M.-A. Badet-Denisot, Highlights of glucosamine-6P synthase catalysis, Arch. Biochem. Biophys. 474 (2008) 302–317.
[9] M.-A. Denisot, F. Le Goffic, B. Badet, Glucosamine-6-phosphate synthase from Escherichia coli yields two proteins upon limited proteolysis: identification of the glutamine amidohydrolase and 2R ketose/aldose isomerase-bearing domains based on their biochemical properties, Arch. Biochem. Biophys. 288 (1991) 225–230.
[10] J. Raczynska, J. Olchowy, P.V. Konariev, D.I. Svergun, S. Milewski, W. Rypniewski, The crystal and solution studies of glucosamine-6-phosphate synthase from Candida albicans, J. Mol. Biol. 372 (2007) 672–688.
[11] A. Teplyakov, G. Obmolova, M. Badet-denisot, B. Badet, The mechanism of sugar phosphate isomerization by glucosamine 6-phosphate synthase, Protein Sci. 8 (1999) 596–602.
[12] A. Miszkiel, M. Wojciechowski, S. Milewski, Long range molecular dynamics study of regulation of eukaryotic glucosamine-6-phosphate synthase activity by UDP-GlcNAc, J. Mol. Model. 17 (2011) 3103–3115.
[13] D. Van Der Spoel, E. Lindahl, B. Hess, G. Groenhof, A.E. Mark, H.J.C. Berendsen, GROMACS: fast, flexible, and free, J. Comput. Chem. 26 (2005) 1701–1718.
[14] B. Hess, C. Kutzner, D. van der Spoel, E. Lindahl, GROMACS 4: algorithms for highly efficient, load-balanced, and scalable molecular simulation, J. Chem. Theory Comput. 4 (2008) 435–447.
[15] H.J.C. Berendsen, J.P.M. Postma, W.F. Vangunsteren, A. Dinola, J.R. Haak, Molecular-dynamics with coupling to an external bath, J. Chem. Phys. 81 (1984) 3684–3690.
[16] T. Darden, D. York, L. Pedersen, Particle mesh ewald – an N.Log(N) method for ewald sums in large systems, J. Chem. Phys. 98 (1993) 10089–10092.
[17] B. Hess, H. Bekker, H.J.C. Berendsen, J.G.E.M. Fraaije, LINCS. a linear constraint solver for molecular simulations, J. Comput. Chem. 18 (1997) 1463–1472.
[18] A.W. Schuttelkopf, D.M.F. van Aalten, PRODRG: a tool for high-throughput crystallography of protein-ligand complexes, Acta Crystallogr. Sect. D—Biological Crystallogr. 60 (2004) 1355–1363.
[19] J. Raczynska, J. Olchowy, P.V. Konariev, D.I. Svergun, S. Milewski, W. Rypniewski, The crystal and solution studies of glucosamine-6-phosphate synthase from Candida albicans, J. Mol. Biol. 372 (2007) 672–688.
[20] B. Hess, Similarities between principal components of protein dynamics and random diffusion, Phys. Rev. E 62 (2000) 8438–8448.
[21] B. Hess, Convergence of sampling in protein simulations, Phys. Rev. E 65 (2002) 1–10.
[22] S. Mouilleron, M.-A.A. Badet-Denisot, B. Golinelli-Pimpaneau, Ordering of C-terminal loop and glutaminase domains of glucosamine-6-phosphate synthase promotes sugar ring opening and formation of the ammonia channel, J. Mol. Biol. 377 (2008) 1174–1185.
[23] A.K. Bera, J.L. Smith, H. Zalkin, Dual role for the glutamine phosphoribosylpyrophosphate amidotransferase ammonia channel – interdomain signaling and intermediate channeling, J. Biol. Chem. 275 (2000) 7975–7979.
[24] J. Olchowy, I. Gabriel, S. Milewski, Functional domains and interdomain communication in Candida albicans glucosamine-6-phosphate synthase, Biochem. J. 404 (2007) 121–130.